

# Unveiling the Active Structure of Single Nickel Atom Catalysis: Critical Roles of Charge Capacity and Hydrogen Bonding

Xunhua Zhao and Yuanyue Liu\*



Cite This: *J. Am. Chem. Soc.* 2020, 142, 5773–5777



Read Online

ACCESS |



Metrics & More

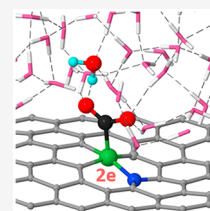


Article Recommendations



Supporting Information

**ABSTRACT:** A single nickel atom embedded in graphene is one of the most representative single-atom catalysts, and it has a high activity and selectivity for electrochemical CO<sub>2</sub> reduction (CO<sub>2</sub>R) to CO. However, the catalytic origin, especially the coordination structure of Ni, remains highly puzzling, as previous density functional theory (DFT) calculations showed that all the possible structures should be inactive and/or nonselective. Here, using *ab initio* molecular dynamics (AIMD) and a “slow-growth” sampling approach to evaluate the reaction kinetic barriers, we show that the charge capacity (of the site) and hydrogen bonding (with the intermediates), which were neglected/oversimplified in previous DFT calculations, play crucial roles, and including their effects can resolve the catalytic origin. Particularly, a high charge capacity allows the catalytic site to carry more charges than required for the electrochemical step, lowering the electrochemical barrier, and hydrogen bonding promotes the reaction that produces polar intermediates by stabilizing the intermediates and facilitating the H transfer from water, explaining the high selectivity for CO<sub>2</sub>R over the hydrogen evolution reaction. Consequently, we find that a hybrid coordination environment (with one nitrogen and three carbon atoms) for the Ni-atom is most active and selective for CO<sub>2</sub>R. Our work not only explains a long-standing puzzle for an important catalyst but also highlights the crucial roles of charge capacity and hydrogen bonding, which can help elucidate the mechanisms of other heterogeneous electrocatalysts in aqueous solution and enable more effective catalyst design.



## INTRODUCTION

Single-atom catalysis<sup>1</sup> is an important type of catalysis and has demonstrated promising performance for many reactions,<sup>2–6</sup> such as the electrochemical carbon dioxide reduction (CO<sub>2</sub>R) reaction, which converts exhaust carbon source into valuable fuels and chemicals and is considered as a promising technique for a carbon-neutral economy.<sup>7</sup> A representative single-atom catalyst is the single nickel atom embedded in nitrogen-doped graphene, which has high activity and selectivity for carbon dioxide reduction to CO<sup>8–12</sup> in aqueous solution. However, its catalytic mechanism remains elusive; particularly, there is much debate over the coordination structure of the Ni-atom. Figure 1 shows the commonly studied structures, where the Ni-atom can be bonded with three or four atoms, with different combinations of C and N. The reaction energies and the intermediates of these structures have been studied in many publications<sup>2,9,12,13</sup> using density functional theory (DFT) calculations based on the widely used “Computational Hydrogen Electrode” (CHE) model.<sup>14</sup> However, a careful examination of the calculation results finds that none of the proposed structures is active and/or selective. For example, Yang et al.<sup>12</sup> proposed that four-N-atom-coordinated Ni (referred to as the “4N” site in this article) is responsible for the high activity and selectivity; however, their DFT results showed a rather high formation energy (>1.7 eV) for the \*COOH (a critical intermediate of CO<sub>2</sub>R), indicating that this site should not be active. Moreover, their DFT calculations failed to reproduce the chemisorbed CO<sub>2</sub> (\*CO<sub>2</sub>), while their own experiments found the \*CO<sub>2</sub> during the CO<sub>2</sub>R. The 4N

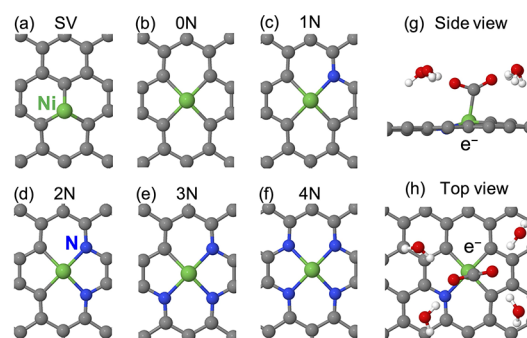


**Figure 1.** (a–f) Possible coordination structures of a single Ni-atom anchored in graphene, which have been commonly considered in the literature. (g, h) Side and top views of a chemisorbed CO<sub>2</sub> stabilized by H<sub>2</sub>O molecules and surface charge. The nickel, nitrogen, carbon, hydrogen, and oxygen atoms are denoted as green, blue, gray, white, and red spheres, respectively.

site is also suggested in other reports,<sup>8,9,15</sup> despite the high formation energy of \*COOH on this site; furthermore, the DFT calculations in those works show that the hydrogen

Received: December 26, 2019

Published: March 3, 2020

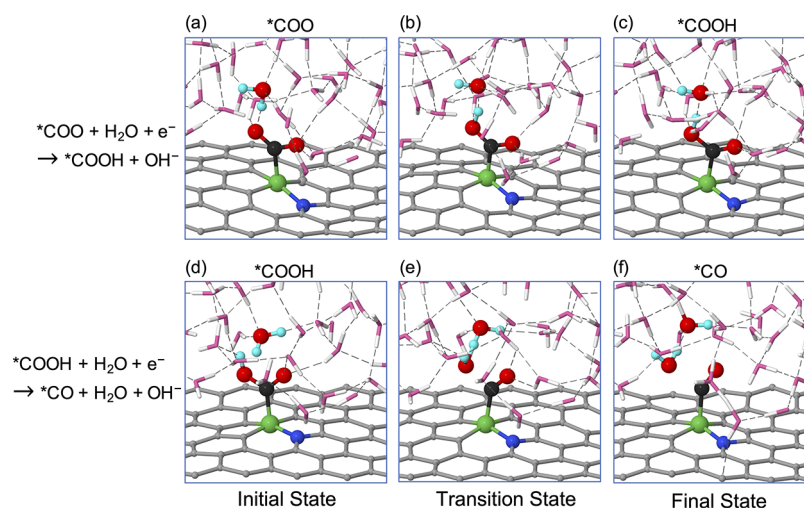


**Figure 2.** Reaction pathway for the  $*\text{COOH}$  formation and  $*\text{CO}$  formation on the 1N site. The Ni, N, and the species directly involved in the reaction are shown by spheres (Ni, green; C, black; O, red; H, cyan). Hydrogen bonds are represented by thin dashed lines.

evolution reaction (HER) is more favorable than the  $\text{CO}_2\text{R}$ , contradicting the experimental observation of high selectivity for  $\text{CO}_2\text{R}$ .<sup>8,9,15</sup> Jiang et al.<sup>13,16</sup> proposed that three-C-atom-coordinated Ni (which can also be thought of as Ni being embedded in a single vacancy of graphene, and therefore is referred to as the “SV” site in this report) is responsible for  $\text{CO}_2\text{R}$ , as it has a lower formation energy of  $*\text{COOH}$ . However, the DFT calculations show that this site still prefers HER over  $\text{CO}_2\text{R}$  and does not adsorb  $\text{CO}_2$  chemically, both of which are in contradiction to experimental results. Overall, the DFT calculations suggest that none of the proposed structures is active and/or selective.

## METHODS

These DFT calculations are based on the CHE model. Although this model is simple and has been widely used for a variety of electrochemical reactions, it neglects/oversimplifies several factors that can be important: (1) The CHE model assumes zero charge on the catalyst surface before the reaction; however, in reality, the catalyst often has nonzero surface charge, which can affect the chemical reactivity.<sup>17</sup> (2) Moreover, the chemical interactions between the reaction intermediate adsorbed on the catalyst and the surrounding solvent molecules are often neglected; these interactions can be strong, particularly for reactions in aqueous solution when the intermediate contains a highly charged atom that can form hydrogen bond(s) with water.<sup>18</sup> (3) The CHE considers only thermodynamics, while the information on kinetics (e.g., transition-state barrier) is also important.<sup>19,20</sup> Note that an important feature of water solvent is that the hydrogen-bonding network can dynamically change during the reaction, which cannot be captured by the commonly used barrier evaluation method—nudged elastic band—as it relies on “static” configurations.

To overcome these issues of the CHE model, here we explicitly include the surface charge (determined by the applied electrode potential) and several layers of water in the simulation. To evaluate the kinetic barriers, we use *ab initio* molecular dynamics (AIMD) with a “slow-growth” method<sup>21–23</sup> to sample the free energy profile. This approach also allows us to capture the varying H-bonding network during the reaction. We consider six possible active sites that are commonly studied in literature, as shown in Figure 1, which are referred as  $x\text{N}$  (where  $x = 0, 1, 2, 3, 4$  is the number of N-atoms coordinated with the Ni-atom embedded in a divacancy) and SV. The computation details can be found in the Supporting Information (SI).

## RESULTS AND DISCUSSIONS

First, we find that the surface charge and hydrogen bonding together can lead to chemisorption of  $\text{CO}_2$ , while without either of them, the  $\text{CO}_2$  is weakly physisorbed (see Table S2 and the related text in the SI). This finding explains why previous DFT calculations failed to reproduce the experimentally observed chemisorbed  $\text{CO}_2$ —due to the neglect of the surface charge and hydrogen bonding. Taking the 1N site as an example, with one negative surface charge (produced by adding one extra electron into the system) and the presence of four water molecules, the  $\text{CO}_2$  is bent and adsorbed on Ni (the C–Ni distance is  $<2 \text{ \AA}$ ), meanwhile forming four hydrogen bonds with the surrounding  $\text{H}_2\text{O}$  molecules (the H–O distance ranges from 1.76 to 1.86  $\text{ \AA}$ ), as shown in Figure 1g,h. When the surface charge or  $\text{H}_2\text{O}$  molecules are removed, the  $\text{CO}_2$  will detach from the Ni (C–N distance becomes  $>3 \text{ \AA}$ ) and restore the linear configuration. The chemisorbed  $\text{CO}_2$  is also found to be stable, and multiple H-bonds are always present throughout our AIMD simulations with more  $\text{H}_2\text{O}$  molecules (72 in total). These results suggest the crucial effects of surface charge and H-bonding, which should be included when studying aqueous electrocatalysis.

With the confirmation of the chemisorbed  $\text{CO}_2$  as an intermediate in the  $\text{CO}_2\text{R}$  on a single Ni-atom, we next explored the energy and structural evolution of a sequential reaction path. We considered the following three steps that can take place in a neutral or alkaline environment (where most experiments are performed): (1)  $*\text{COO} + \text{H}_2\text{O} + e^- \rightarrow * \text{COOH} + \text{OH}^-(\text{aq})$ , referred to as the  $*\text{COOH}$  formation step; (2)  $*\text{COOH} + \text{H}_2\text{O} + e^- \rightarrow * \text{CO} + \text{H}_2\text{O} + \text{OH}^-(\text{aq})$ , referred to as the  $*\text{CO}$  formation step; and (3)  $*\text{CO} \rightarrow \text{CO}(\text{aq})$ , referred to as the CO desorption step. The first two steps are electrochemical steps, while the last one is a thermal step (no electrons involved explicitly). Note that the 4N site cannot chemically adsorb CO, and thus the last two steps on the 4N site combine into a single step:  $*\text{COOH} + \text{H}_2\text{O} + e^- \rightarrow \text{CO}(\text{aq}) + \text{H}_2\text{O} + \text{OH}^-(\text{aq})$ . Representative snapshots of the structural evolution during electrochemical steps on the 1N site are shown in Figure 2. Again, we find multiple hydrogen bonds between the intermediates ( $*\text{COO}$  and  $*\text{COOH}$ ) and the solvent  $\text{H}_2\text{O}$  molecules in all the snapshots. The  $\text{OH}^-$  generated in the electrochemical steps forms a complex

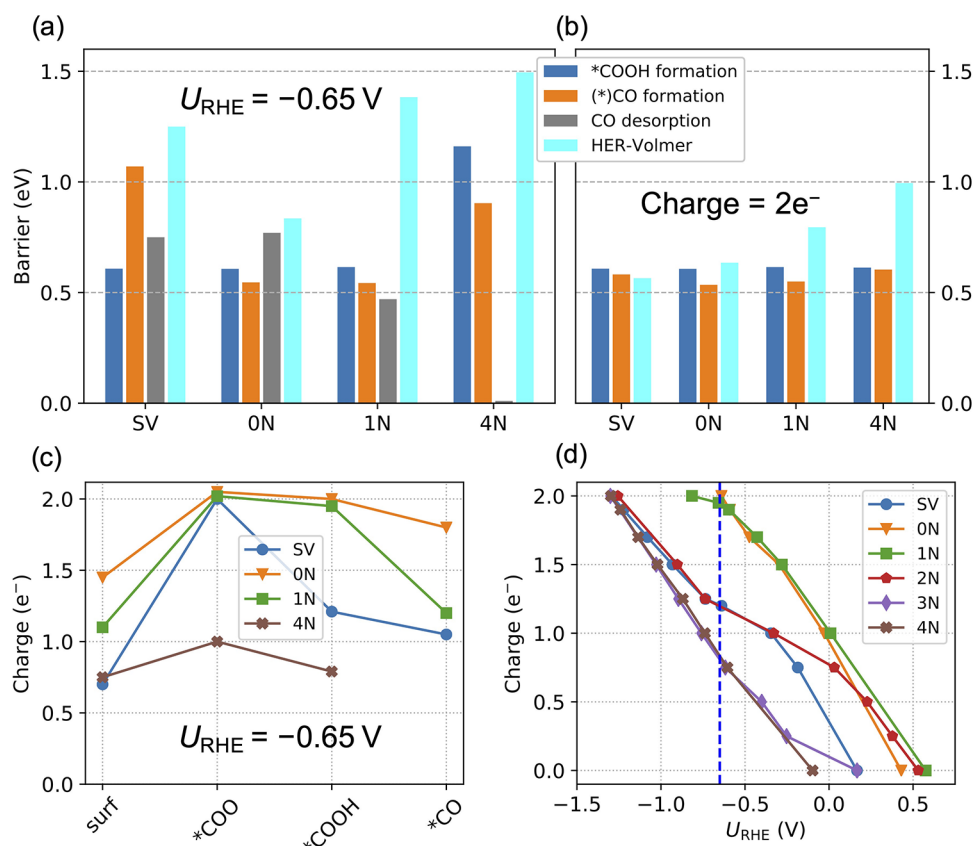


**Figure 3.** Kinetic barriers for conditions (a)  $U_{RHE} = -0.65$  V and (b) charge =  $2e^-$ . (c) Charge capacity at  $U_{RHE} = -0.65$  V for different sites with different adsorbates. (d) Charge capacity dependence on the potential for \*COOH at different sites.

(typically  $H_3O_2^-$ ) with neighboring  $H_2O$  molecule(s) and diffuses away from the site through a hydrogen-bonding network. Note that the \*CO formation step involves simultaneous decomposition and formation of  $H_2O$  molecules: one  $H_2O$  donates its H to OH in \*COOH, to form  $OH^-$  and a new  $H_2O$ .

Figure 3a shows the kinetic barriers for different steps on different sites under a potential of  $-0.65$  V vs RHE ( $U_{RHE} = -0.65$  V, at which a significant amount of CO is produced experimentally). The 0N and 1N sites are found to have lower barriers for electrochemical steps than 4N and SV sites. Specifically, the SV site has a high barrier for the \*CO formation step (1.07 eV), and the 4N site has a high barrier for the \*COOH formation step (1.16 eV), indicating that these sites are inactive for the  $CO_2R$  at  $U_{RHE} = -0.65$  V. In contrast, the 0N and 1N sites have much lower barriers for the electrochemical steps (0.61 and 0.62 eV for \*COOH formation; 0.54 and 0.55 eV for \*CO formation). Interestingly, both sites have similar barriers for the electrochemical steps (which will be explained later). The activity difference between the 0N and 1N sites is determined by the CO desorption barrier: 0.77 eV for 0N and 0.47 eV for 1N; thus, the 1N site has a higher activity for  $CO_2R$ . Although here we did not explicitly calculate the barriers for the 2N and 3N sites, our later analyses suggest that these sites should have high barriers for electrochemical steps. Therefore, we conclude that the 1N site is the most active for  $CO_2R$ . Note that previous DFT calculations based on the CHE model showed that the 1N site is inactive, with an onset overpotential magnitude  $>1$  V,<sup>13</sup> due to the oversimplifications in the CHE model, as discussed in the Methods section.

What determines the difference in electrochemical barriers across different sites? Why do 0N and 1N sites have lower barriers for electrochemical steps than 4N and SV sites? Why do 0N and 1N sites have similar electrochemical barriers? All these can be explained by the number of charges that the site can carry, i.e., the charge capacity. As shown in Figure 3c, at  $U_{RHE} = -0.65$  V, the 0N, 1N, and SV sites with \*CO $_2$  have  $\sim 2$  negative charges ( $2e^-$ ), while the 4N site has only less than  $1e^-$ . Since the excessive negative charges accumulated at the site can facilitate the charge transfer for the sequential electrochemical step, the 0N, 1N, and SV sites with \*COO thus have lower barriers for the sequential \*COOH formation step than 4N. Note that 0N, 1N, and SV have similar barriers for \*COOH formation, which is consistent with their similar charge capacity (with \*COO). After the \*COOH is formed, the 0N and 1N sites can still have  $\sim 2$  e $^-$ , while the charge capacity of the SV site drops to  $\sim 1.2$  e $^-$ , giving rise to its large barrier for the sequential step—\*CO formation. Although high charge capacity can benefit the electrochemical step, it may impede the desorption step. This can be seen from the difference in CO desorption barriers between the 0N and 1N sites. Even though they have similar barriers in the charge-neutral state, under  $U_{RHE} = -0.65$  V, the 0N site has more charges than the 1N site (0N vs 1N: 1.8 vs 1.2 e $^-$ ), giving rise to a stronger binding with CO (1.03 vs 0.76 eV) and thus a higher desorption barrier (Figure 3a: 0.77 vs 0.47 eV). These results suggest that the charge capacity plays a key role in determining the activity of the site/catalyst—a large charge capacity will lower the barrier for the electrochemical step, while too large a capacity may impede the desorption, and thus an optimal charge capacity is desired for high catalytic activity.

To further confirm the role of the charge capacity, we calculate the electrochemical barriers for different sites with the same number of surface charge. As shown in Figure 3b, we find that the barriers of \*COOH formation (or (\*CO formation) become similar for different sites. For example, when the 4N site is charged with  $2e^-$  for the \*COOH formation step, its barrier is lowered to 0.61 eV, similar to that on the 0N/1N site. These results also suggest that when the potential is sufficiently high that the 4N site has enough surface charge, it will become active. Our calculations show that, in order to activate the 4N site, the  $U_{\text{RHE}}$  needs to be  $< -1.2$  V. Similarly, when the SV site is charged with  $2e^-$  for the \*CO formation step, its barrier is also lowered to 0.60 eV, comparable with that on the 0N/1N site. Note that under these potentials, the 0N and 1N sites would have more surface charges, and thus they are still more active (toward \*CO) than 4N and SV.

Why do 0N and 1N have a higher charge capacity than 4N and SV? Figure 3d shows the number of surface charges as a function of the applied electrode potential for the sites, with \*COOH as an example. When the potential becomes more negative, the number of surface charges increases, and the derivative of this charge–potential curve defines the (differential) capacitance. Although the 4N site has a capacitance similar to those of 0N and 1N, it has a higher Fermi level (lower work function) at the charge-neutral state; therefore, when it is charged to the same final Fermi level (defined by the applied electrode potential) as the 0N and 1N, it has fewer surface charges, i.e., lower capacity. Similarly, the SV site also has a higher Fermi level than 0N and 1N at the charge-neutral state; moreover, its differential capacitance decreases during charging; therefore, it also has a lower capacity than 0N and 1N. Besides the work function at the charge-neutral state, the density of states can also affect the charge capacity, although its role is not as clear as that of the work function (see Figure S4 and the related text in the SI). Figure 3d also shows the charge capacities of the 2N and 3N sites at  $U_{\text{RHE}} = -0.65$  V: the 2N site has the same capacity as the SV site, and the 3N site has the same capacity as the 4N site. Since they both have lower charge capacity than the 0N and 1N sites, they should have higher electrochemical barriers and thus be less active.

Our calculations also show that the 0N and 1N sites prefer  $\text{CO}_2\text{R}$  over HER (Figure 3), explaining the origin of the experimentally observed selectivity. For example, on the 1N, at  $U_{\text{RHE}} = -0.65$  V, the first step of the HER—Volmer reaction— $\text{H}_2\text{O} + e^- \rightarrow *H + \text{OH}^-(\text{aq})$ —already requires a barrier of 1.38 eV, while the first step of the  $\text{CO}_2\text{R}$  reaction— $\text{CO}_2$  chemisorption—is barrierless, and the sequential steps have barriers  $< 0.65$  eV. Compared with  $\text{CO}_2$  chemisorption, whose product (\*COO) is stabilized by multiple hydrogen bonds, the Volmer step creates a H adsorbed on Ni, which is nearly charge neutral and thus cannot form H bonds with water. (Using the Bader partition method,<sup>24</sup> we find that the H adsorbed on Ni has only  $+0.07$  e charge, much less than the H in water:  $+1$  e.) The H bonding not only helps stabilize the \*COO but also facilitates the sequential  $\text{CO}_2\text{R}$  electrochemical steps that involve H donation by bringing the  $\text{H}_2\text{O}$  close to the intermediates (\*COO and \*COOH). In contrast, for HER, the distance between H in  $\text{H}_2\text{O}$  and the Ni is  $> 2.5$  Å due to the lack of H bonding. In addition to the H-bonding effects, the charge capacity may also play a role: the Volmer step starts from a bare site (without any adsorbate), while the electrochemical steps of the  $\text{CO}_2\text{R}$  start from a site with adsorbates; as shown in Figure 3c, the adsorbates can increase

the charge capacity, which helps lower the electrochemical steps and may be one of the reasons for the lower electrochemical barriers of  $\text{CO}_2\text{R}$  compared with the Volmer step. Thanks to the above reasons, the kinetic barrier for HER is significantly higher than for  $\text{CO}_2\text{R}$ , and consequently  $\text{CO}_2\text{R}$  selectivity can reach as high as 99% in experiments.<sup>8,11</sup>

Although this work focuses on single-Ni-atom catalysts, it is interesting to compare with other single-metal-atom catalysts such as Fe, Co, and Cu. To do so, ideally we should calculate the kinetic barrier for each step on all the possible sites of different metal atoms,  $M-x\text{N}$  (where  $M = \text{Fe}, \text{Co}, \text{Cu}; x = 0, 1, 2, 3, 4$ ), similar to what we have done for  $\text{Ni}-x\text{N}$ . However, the high computational cost of our method prevents us from obtaining the full set of barriers in this work. Nevertheless, we can use the charge capacities and the CO binding energies to qualitatively compare other  $M-x\text{N}$  with the Ni-1N site. We first consider the electrochemical steps using the CO formation step as an example. As shown in Table S1 in the SI, compared with the Ni-1N (with COOH) that carries  $\sim 2 e^-$ , only Fe/Co-0/1/2N and Cu-0N can carry similar charges, while the others have lower charges and thus are likely to have higher barriers for electrochemical steps. Then, for Fe/Co-0/1/2N and Cu-0N sites, we consider the thermal step, i.e., CO desorption, by comparing the CO binding energies with that of Ni-1N. It is found that the CO are strongly bound on Fe/Co-0/1/2N ( $> 1.5$  eV; for comparison, the CO binding energy on Ni-1N is only  $\sim 0.7$  eV), hindering the CO desorption, while the CO binding energy on Cu-0N is  $\sim 0.2$  eV. Our results suggest that the single Fe- and Co-atoms are not as active as Ni, which agrees with the experimental observations.<sup>15</sup> They also suggest that the low performance of single Cu-atoms may be due to a low density of active sites.

## CONCLUSION

In summary, we unveiled the catalytic origin of the single Ni-atom in N-doped graphene for electrochemical  $\text{CO}_2$  reduction to CO in water, which was puzzling, as all previous DFT calculations suggested that it should not be active and/or selective. We found that the excessive charge on the catalyst, quantified by charge capacity, can significantly facilitate the electrochemical steps, and the hydrogen bonding promotes the reaction that produces polar intermediates by stabilizing the intermediates and facilitating the H transfer from water. As a result, the 1N site has the highest activity and selectivity for  $\text{CO}_2\text{R}$ . Our work reveals/highlights the critical roles of the charge capacity and hydrogen bonding in aqueous electrochemical reactions and paves a way toward improved understanding and effective design of catalysts.

## ASSOCIATED CONTENT

### Supporting Information

The Supporting Information is available free of charge at <https://pubs.acs.org/doi/10.1021/jacs.9b13872>.

Computation details; functional dependence of CO adsorption; charge capacity comparison for other transition metal sites; density of states comparison; adsorption energy of  $\text{CO}_2$  with/without  $\text{H}_2\text{O}$  molecules, and with/without charge; effects of water molecules on the charge capacity (PDF)

## ■ AUTHOR INFORMATION

## Corresponding Author

Yuanyue Liu – Texas Materials Institute and Department of Mechanical Engineering, The University of Texas at Austin, Austin, Texas 78712, United States; [orcid.org/0000-0002-5880-8649](https://orcid.org/0000-0002-5880-8649); Email: [yuanyue.liu@austin.utexas.edu](mailto:yuanyue.liu@austin.utexas.edu)

## Author

Xunhua Zhao – Texas Materials Institute and Department of Mechanical Engineering, The University of Texas at Austin, Austin, Texas 78712, United States

Complete contact information is available at:  
<https://pubs.acs.org/10.1021/jacs.9b13872>

## Notes

The authors declare no competing financial interest.

## ■ ACKNOWLEDGMENTS

This work is supported by the National Science Foundation (Grant No. 1900039) and the Welch Foundation (Grant No. F-1959-20180324). This work used computational resources at (1) National Renewable Energy Lab (sponsored by the DOE's Office of EERE), (2) the Extreme Science and Engineering Discovery Environment (XSEDE) through allocation TG-CHE190065, (3) the Center for Nanoscale Materials (a DOE Office of Science user facility supported under Contract No. DE-AC02-06CH11357) at Argonne National Lab, and (4) the Center for Nanophase Materials Sciences (a DOE Office of Science user facility) at Oak Ridge National Laboratory.

## ■ REFERENCES

- (1) Wang, A.; Li, J.; Zhang, T. Heterogeneous Single-Atom Catalysis. *Nat. Rev. Chem.* **2018**, *2* (6), 65–81.
- (2) Zhao, X.; Shi, J.; Ji, Y.; Liu, Y. The Electronic Structure Underlying Electrocatalysis of Two-dimensional Materials. *Wiley Interdiscip. Rev.: Comput. Mol. Sci.* **2019**, *9* (6), e1418.
- (3) Su, X.; Yang, X.-F.; Huang, Y.; Liu, B.; Zhang, T. Single-Atom Catalysis toward Efficient CO<sub>2</sub> Conversion to CO and Formate Products. *Acc. Chem. Res.* **2019**, *52* (3), 656–664.
- (4) Liu, X.; Jiao, Y.; Zheng, Y.; Jaroniec, M.; Qiao, S.-Z. Building Up a Picture of the Electrocatalytic Nitrogen Reduction Activity of Transition Metal Single-Atom Catalysts. *J. Am. Chem. Soc.* **2019**, *141* (24), 9664–9672.
- (5) Yang, L.; Cheng, D.; Xu, H.; Zeng, X.; Wan, X.; Shui, J.; Xiang, Z.; Cao, D. Unveiling the High-Activity Origin of Single-Atom Iron Catalysts for Oxygen Reduction Reaction. *Proc. Natl. Acad. Sci. U. S. A.* **2018**, *115* (26), 6626.
- (6) Xu, H.; Cheng, D.; Cao, D.; Zeng, X. A Universal Principle for a Rational Design of Single-Atom Electrocatalysts. *Nat. Catal.* **2018**, *1* (5), 339–348.
- (7) Chu, S.; Cui, Y.; Liu, N. The Path towards Sustainable Energy. *Nat. Mater.* **2017**, *16* (1), 16–22.
- (8) Bi, W.; Li, X.; You, R.; Chen, M.; Yuan, R.; Huang, W.; Wu, X.; Chu, W.; Wu, C.; Xie, Y. Surface Immobilization of Transition Metal Ions on Nitrogen-Doped Graphene Realizing High-Efficient and Selective CO<sub>2</sub> Reduction. *Adv. Mater.* **2018**, *30* (18), 1706617.
- (9) Li, X.; Bi, W.; Chen, M.; Sun, Y.; Ju, H.; Yan, W.; Zhu, J.; Wu, X.; Chu, W.; Wu, C.; Xie, Y. Exclusive Ni–N 4 Sites Realize Near-Unity CO Selectivity for Electrochemical CO<sub>2</sub> Reduction. *J. Am. Chem. Soc.* **2017**, *139* (42), 14889–14892.
- (10) Bi, W.; Wu, C.; Xie, Y. Atomically Thin Two-Dimensional Solids: An Emerging Platform for CO<sub>2</sub> Electroreduction. *Acs Energy Lett.* **2018**, *3* (3), 624–633.
- (11) Liu, S.; Yang, H. B.; Hung, S.-F.; Ding, J.; Cai, W.; Liu, L.; Gao, J.; Li, X.; Ren, X.; Kuang, Z.; Huang, Y.; Zhang, T.; Liu, B. Elucidating the Electrocatalytic CO<sub>2</sub> Reduction Reaction over a Model Single-Atom Nickel Catalyst. *Angew. Chem., Int. Ed.* **2020**, *59* (2), 798–803.
- (12) Yang, H.; Hung, S.-F.; Liu, S.; Yuan, K.; Miao, S.; Zhang, L.; Huang, X.; Wang, H.-Y.; Cai, W.; Chen, R.; Gao, J.; Yang, X.; Chen, W.; Huang, Y.; Chen, H.; Li, C.; Zhang, T.; Liu, B. Atomically Dispersed Ni(i) as the Active Site for Electrochemical CO<sub>2</sub> Reduction. *Nat. Energy* **2018**, *3* (2), 140–147.
- (13) Jiang, K.; Siahrostami, S.; Akey, A. J.; Li, Y.; Lu, Z.; Lattimer, J.; Hu, Y.; Stokes, C.; Gangishetty, M.; Chen, G.; Zhou, Y.; Hill, W.; Cai, W.; Bell, D.; Chan, K.; Nørskov, J.; Cui, Y.; Wang, H. Transition-Metal Single Atoms in a Graphene Shell as Active Centers for Highly Efficient Artificial Photosynthesis. *Chem.* **2017**, *3* (6), 950–960.
- (14) Nørskov, J.; Rossmeisl, J.; Logadottir, A.; Lindqvist, L.; Kitchin, J.; Bligaard, T.; Jónsson, H. Origin of the Overpotential for Oxygen Reduction at a Fuel-Cell Cathode. *J. Phys. Chem. B* **2004**, *108* (46), 17886–17892.
- (15) Ju, W.; Bagger, A.; Hao, G.-P.; Varela, A.; Sinev, I.; Bon, V.; Cuenya, B. R.; Kaskel, S.; Rossmeisl, J.; Strasser, P. Understanding Activity and Selectivity of Metal-Nitrogen-Doped Carbon Catalysts for Electrochemical Reduction of CO<sub>2</sub>. *Nat. Commun.* **2017**, *8* (1), 944.
- (16) Jiang, K.; Siahrostami, S.; Zheng, T.; Hu, Y.; Hwang, S.; Stavitski, E.; Peng, Y.; Dynes, J.; Gangishetty, M.; Su, D.; Attenkofer, K.; Wang, H. Isolated Ni Single Atoms in Graphene Nanosheets for High-Performance CO<sub>2</sub> Reduction. *Energy Environ. Sci.* **2018**, *11* (4), 893–903.
- (17) Kim, D.; Shi, J.; Liu, Y. Substantial Impact of Charge on Electrochemical Reactions of Two-Dimensional Materials. *J. Am. Chem. Soc.* **2018**, *140* (29), 9127–9131.
- (18) Cheng, T.; Fortunelli, A.; Goddard, W. A. Reaction Intermediates during Operando Electrocatalysis Identified from Full Solvent Quantum Mechanics Molecular Dynamics. *Proc. Natl. Acad. Sci. U. S. A.* **2019**, *116* (16), 7718–7722.
- (19) Cheng, T.; Xiao, H.; Goddard, W. A. Reaction Mechanisms for the Electrochemical Reduction of CO<sub>2</sub> to CO and Formate on the Cu(100) Surface at 298K from Quantum Mechanics Free Energy Calculations with Explicit Water. *J. Am. Chem. Soc.* **2016**, *138* (42), 13802–13805.
- (20) Lindgren, P.; Kastlunger, G.; Peterson, A. A. A Challenge to the G ~ 0 Interpretation of Hydrogen Evolution. *ACS Catal.* **2020**, *10*, 121–128.
- (21) Woo, T. K.; Margl, P. M.; Blöchl, P. E.; Ziegler, T. A Combined Car–Parrinello QM/MM Implementation for Ab Initio Molecular Dynamics Simulations of Extended Systems: Application to Transition Metal Catalysis. *J. Phys. Chem. B* **1997**, *101* (40), 7877–7880.
- (22) Jarzynski, C. Nonequilibrium Equality for Free Energy Differences. *Phys. Rev. Lett.* **1997**, *78* (14), 2690–2693.
- (23) Oberhofer, H.; Dellago, C.; Geissler, P. L. Biased Sampling of Nonequilibrium Trajectories: Can Fast Switching Simulations Outperform Conventional Free Energy Calculation Methods? *J. Phys. Chem. B* **2005**, *109* (14), 6902–6915.
- (24) Tang, W.; Sanville, E.; Henkelman, G. A Grid-Based Bader Analysis Algorithm without Lattice Bias. *J. Phys.: Condens. Matter* **2009**, *21* (8), 084204.